International Scholarly Research Network
ISRN Communications and Networking
Volume 2012, Article ID 132465, 11 pages
doi:10.5402/2012/132465

Research Article

A Systematic Approach for the Design, Fabrication, and Testing of Microstrip Antennas Using Inkjet Printing Technology

Yahiea Al-Naiemy,[1] Taha A. Elwi,[2] Haider R. Khaleel,[2] and Hussain Al-Rizzo[2]

[1] *Department of Applied Science, College of Science and Mathematics, University of Arkansas at Little Rock, Little Rock, AR 72204-1099, USA*
[2] *Department of Systems Engineering, George W. Donaghey College of Engineering and Information Technology, University of Arkansas at Little Rock, Little Rock, AR 72204-1099, USA*

Correspondence should be addressed to Yahiea Al-Naiemy, ymainaiemy@ualr.edu

Received 8 February 2012; Accepted 4 April 2012

Academic Editors: C. Luxey, J. Park, H. M. Sun, and K. Teh

We present a systematic approach for producing microstrip antennas using the state-of-the-art-inkjet printing technique. An initial antenna design based on the conventional square patch geometry is adopted as a benchmark to characterize the entire approach; the procedure then could be generalized to different antenna geometries and feeding techniques. For validation purposes, the antenna is designed and simulated using two different 3D full-wave electromagnetic simulation tools: Ansoft's High Frequency Structure Simulator (HFSS), which is based on the Finite Element Method (FEM), and CST Microwave Studio, which is based on the Finite Integration Technique (FIT). The systematic approach for the fabrication process includes the optimal number of printed layers, curing temperature, and curing time. These essential parameters need to be optimized to achieve the highest electrical conductivity, trace continuity, and structural robustness. The antenna is fabricated using Inkjet Printing Technology (IJPT) utilizing Sliver Nanoparticles (SNPs) conductive ink printed by DMP-2800 Dimatix FujiFilm materials printer.

1. Introduction

During the past four decades, microstrip antennas have attracted a great deal of attention due to their low profile, ease of fabrication, low cost, and conformability. Inkjet-printed antennas using highly conducting patterns can complement and extend the above-mentioned advantages to achieve modern, clean, fast, and reliable antenna fabrication technologies. Moreover, the use of nanoscale materials allows for the development of a new generation of modern printed circuit antennas [1–3]. Due to the ever-growing demands for printed RF circuits and antennas to serve different emerging applications such as Radio Frequency Identification (RFID), wireless sensors, portable health monitoring, and wearable devices, several eager attempts from different research groups have been conducted to investigate the use of conductive ink based on different nanostructural materials to explore low-cost roll-to-roll production, improve wireless connectivity, structural performance, and flexibility and to reduce the level of environmental contamination [4–8].

In wireless sensor applications, several RFID designs were reported [9–12] using inkjet technology on low-cost paper substrates. Furthermore, Ultrahigh Frequency (UHF)/RFID printed on flexible, organic, and liquid crystal polymer substrate have been investigated [13]. In [14], a real-time biomedical monitoring system integrated to a wearable RFID-enabled sensor node was reported using conductive SNP ink printed on low-cost textile substrates. A performance comparison of an inverted-F antenna based on nanosilver Inkjet material with respect to identical prototype made of copper was presented in [9]. Printed bow-tie antennas made of conductive paint were manufactured using screen-printing technique and compared to their identical antennas made of copper [15]. Recently, the integration of microstrip antennas, electronic circuits, and sensors to the panels of photovoltaic cells is considered as a promising design approach.

The above-mentioned advantages of the inkjet printing in addition to the wide spectrum of applications involved in

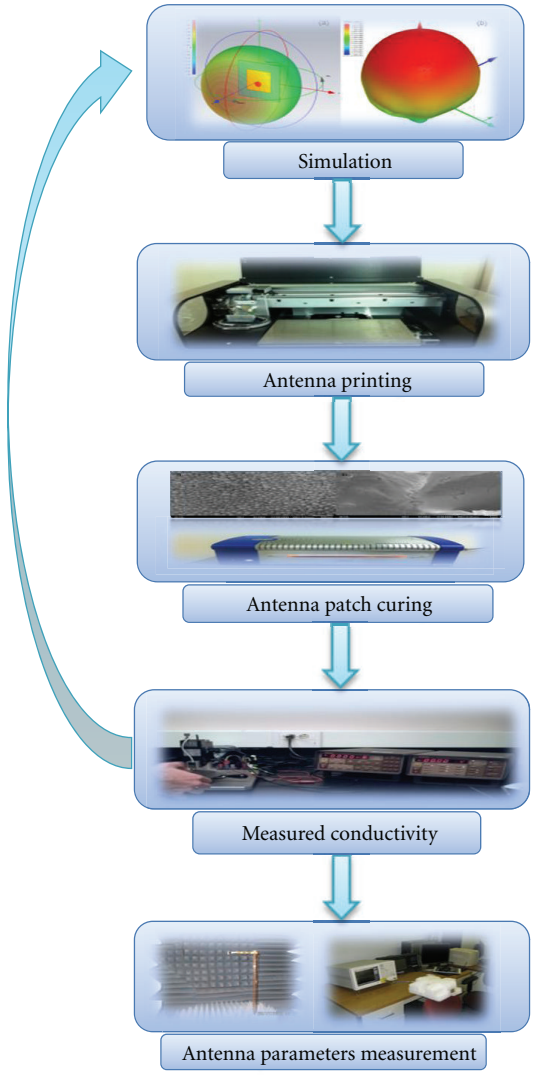

Figure 1: Design and fabrication processes of the prototype antenna.

this technique trigger the need to a procedural literature of the steps involved in microstrip antennas production.

In this paper, a systematic approach for the design, fabrication, and testing of microstrip patch antennas using inkjet printing process is presented. An initial antenna design based on the traditional square patch geometry is involved as a benchmark to characterize the methodology adopted throughout the process. The design and fabrication processes are first presented in Section 2. The printer setup, curing process, and conductivity measurement are presented in Section 3. Section 4 deals with the antenna design and numerical simulation where two different simulation tools based on the Finite Integration Technique (FIT) of CST Microwave Studio [16] and the Finite Element Method (FEM) formulation of Ansoft's High Frequency Structure Simulator (HFSS) [17] are involved to investigate the performance of the antenna under consideration. In Section 5, the fabrication process and measurement are introduced; moreover, the printed antenna prototype is compared against its identical prototype made of copper. Finally, the paper is concluded in Section 6.

2. Design Process and Fabrication

The systematic approach for the design, fabrication, and testing of square patch antenna using IJPT is performed in five stages. The complete design and fabrication processes are schematically illustrated in Figure 1.

As shown in Figure 1, there are five main stages in the proposed approach, namely, simulation, antenna printing, antenna curing, conductivity measurement, and antenna parameters measurements. The design and fabrication processes start with numerical simulation using two different approaches: CST MW and HFSS. After the simulation is performed, printing the patch antennas is carried out with different layers using conductive ink printed using DMP-2800 Dimatix FujiFilm Materials Printer. The optimal fabrication conditions, such as the number of printed layers, curing time, feed structure, and complexity of the printed geometries on different substrates, are discussed. Then, the third stage involves the curing process using high precision convection oven. It is essential to cure the prototype in order to achieve the optimal conductivity of the printed SNP ink. Using the four-probe technique, the DC electrical conductivity of the printed SNP patch is measured. For accurate design parameters, the electrical conductivity measured value of a printed patch sample from this stage is fed to the first stage as seen in the diagram. The fifth stage involves measuring the antenna parameters such as resonant frequency, S_{11}, gain, and far-field radiation patterns.

Finally the simulated and measured parameters of the SNP prototype are compared.

3. Printer Setup, Curing Process, and Conductivity Measurement

3.1. Printer Setup. A Dimatix DMP 2800 Inkjet printer (Fujifilm Dimatix, Inc. Santa Clara, USA) [18] is used to print the antenna geometries using a disposable piezo Inkjet cartridge that contains 16 nozzles of 23 μm diameter spaced 254 μm with typical drop size of 10 pl, drop diameter 27 μm, and capability of jetting 1 pl/10 pl drop.

The DMP printer shown in Figure 2 has 200 mm $\times$ 300 mm printing area with a vacuum platen moving in horizontal direction integrated with fiducial and drop watcher camera and deposition printer with 10 pl nominal drop volume cartridge. The vacuumed platen can be heated up to 60°C. In addition, the wave editor and drop watcher camera allow doctrinaire and control of the electronic pulses to the piezo jetting device to get optimal drop from the nozzles [18]. A piezoelectrical controller is connected to the head of the printer through 16 jets. Additionally the fiducial camera allows taking image capture of printed pattern or drops and cartridge cleaning station to clean the cartridge after each single printing process. The antenna design can be uploaded to the DMP 2800 printer using Dimatix Drop Manager Software in Gerber format file.

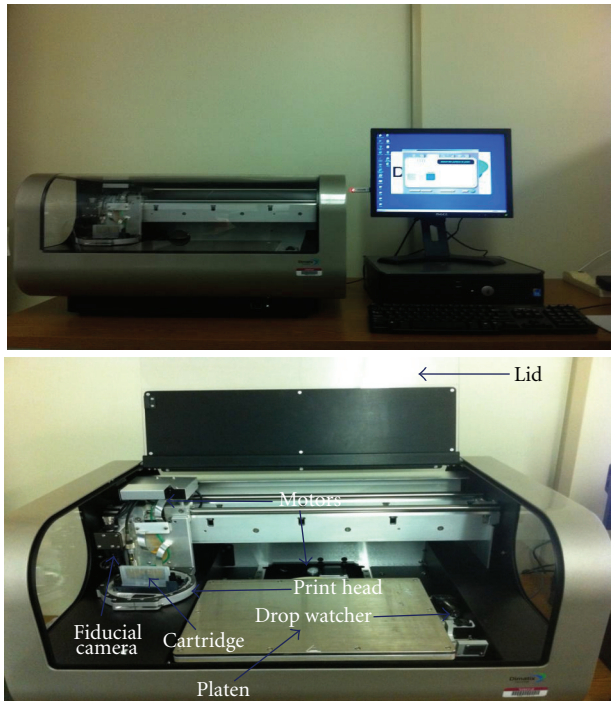

Figure 2: Photograph of Dimatix DMP 2800 inkjet printer with its different parts.

Figure 3: Photograph of the ProtoFlow LPKF's convection oven.

The Gerber file contains all the related geometrical dimensions of the antenna design. Furthermore, all printing processes and the printing setup conditions can be controlled using the Dimatix Drop Manager software such as the number of the printed layers, heating temperature of the platen, number of used jets, and height of the cartridge head with respect to the platen.

Prior to printing the designed antenna, there are several steps that should be taken into account. The substrate must be cleaned and dried; the substrate holder should be preheated to 50°C to accelerate the evaporation of the solvent; the optimization of droplet spacing in the x and y direction is chosen; finally, the distance between the nozzle tip and the substrate and the droplet pitch values should be determined before starting the printing process.

3.2. Curing Process. The printed metal patterns need to be annealed to achieve a high conductivity. Therefore, after printing the SNP patch, a curing process is utilized in order to ensure physical continuity and high electrical conductivity of the printed SNP and to prevent oxidization of the printed surface. The curing process is performed inside the ProtoFlow LPKF's high-precision convection industrial oven as shown in Figure 3, which involves two essential parameters. The annealing temperature and the heating time are fixed with initial values at 120°C and 10 hours, respectively. The conductive ink and printed patterns are heated and burred. A good cure is found after several trials, exposure time control, and different exposure times in order to cure the conductive ink with maximum annealing and minimal deformation of the substrate.

Exposure times of 5, 10, and 30 minutes do not sufficiently dry the solvent. Different durations are used until no deformation of the substrate is observed. The selected initial temperature and heating time are found to be sufficient to enable the onset and development of SNP expansion and grain boundary migration, leading to homogeneity and continuity in the printed SNP structures. The annealing temperature is fixed at 120°C since the maximum temperature that the substrates used, Roger, FR4, can endure is in the range of 120°C to 150°C.

The maximum heating time reported in the literature is 10 hours [19]. We have found that when the heating interval is increased, the SNPs begin to coalesce and the size of the grains increases. The curing process is applied to the printed patches so as to melt the printed SNPs, and good percolation channels are created for electrons to flow as well as to diminish the created cracks due to nanoscale glomeration phenomena [20].

Figure 4 depicts the mechanism of SNP sintering. Figure 4 reveals that the SNP grains reach out to the neighboring grains to form a continuous printed structure with time and temperate curing. Therefore, the cracks and pores on the printed SNP are covered up. In addition to cohesive and adhesive, the printed SNP grains on the substrate are observed in this figure. The curing must be performed immediately after the printing to avoid oxidization, which may lead to conductivity reduction that degrades the antenna efficiency. Images of the printed SNP before and after curing are presented in Figure 4 as obtained from the field emission Scanning Electron Microscope SEM (7000F JEOL Ltd., Tokyo, Japan) with 15 k accelerating voltage. According to the SEM images in Figure 4, it can be observed that an excellent flat surface morphology has been achieved after optimal curing of printed SNPs.

Five samples are printed on 5 mm × 5 mm patches on a Rogers RO 3203 substrate with different heights. Next, the same five patches are reprinted on FR4 and glass substrates for comparison with those printed on the Rogers RO 3203 substrate. In Figure 5 the SEM images provide top view of the printed patches.

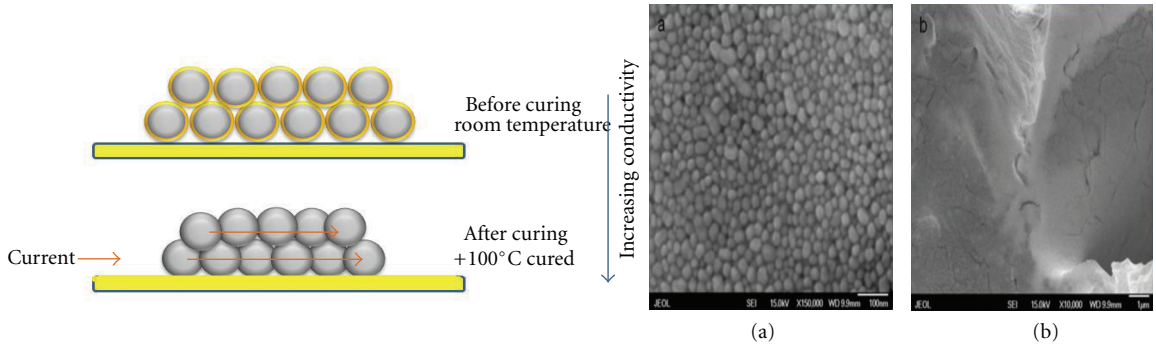

Figure 4: SEM images of a layer of printed nanosilver ink (a) before (b) after curing.

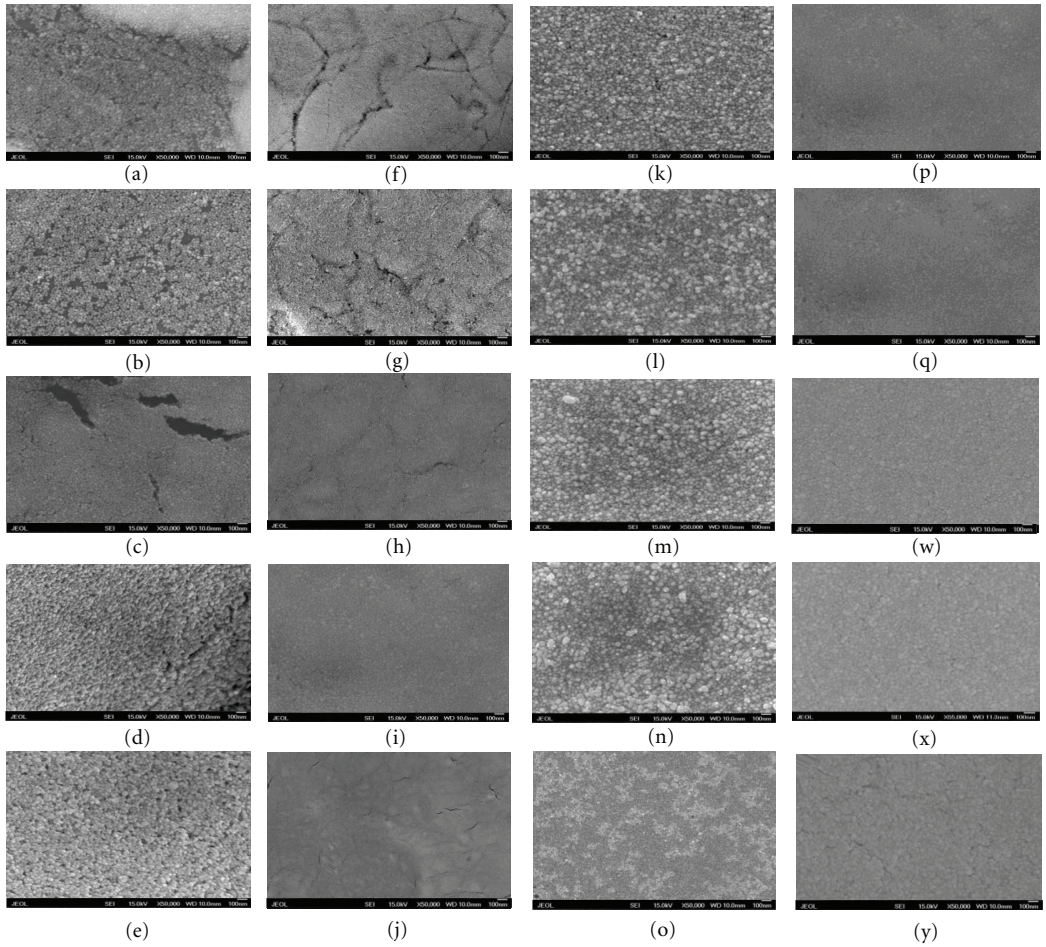

Figure 5: SEM images of the printed SNP patches with different layers ranging from one layer to five layers as shown in (a)–(e) before curing and (f)–(j) after curing for the Rogers RO 3203 substrate, FR4 substrate (k)–(o), and glass substrate (p)–(y).

In general, it is found that the patches printed on the glass substrate appear more homogenous but with less degree of SNP expansion than those printed on Rogers RO 3203 and FR4 substrates and they are without cracks as seen in Figure 5.

However, the cracks in the printed patches on Rogers RO 3203 and FR4 substrates start to diminish with increasing the number of layers as depicted in Figures 5(i) and 5(j) for Rogers RO 3203 substrate and Figures 5(n) and 5(o) for FR4 substrate.

3.3. Conductivity Measurement. To start the design using numerical simulation, the electrical properties of the materials involved in the antenna design must be fully characterized. One such important property is the electrical conductivity. The four-probe conductivity measurement technique

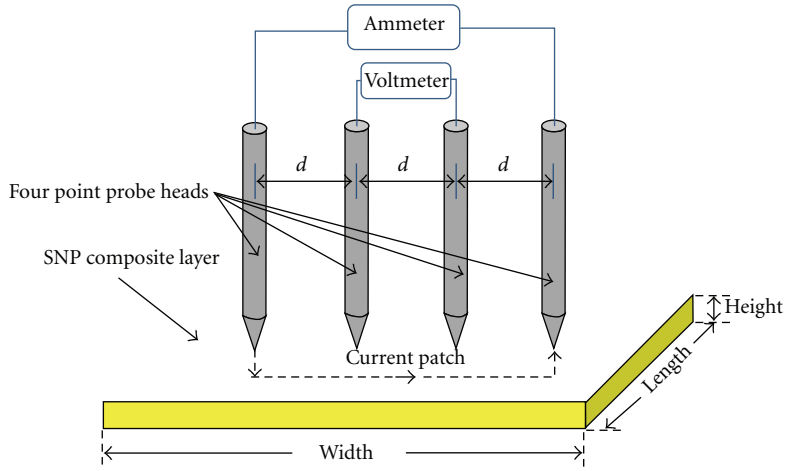

Figure 6: DC conductivity measurement.

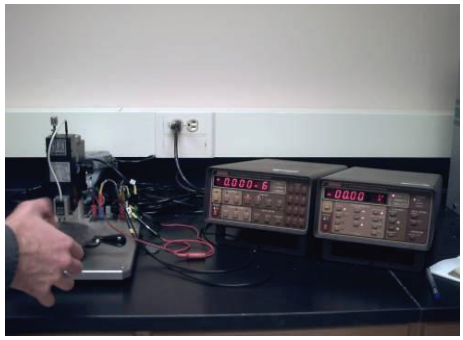

Figure 7: Four-probe (a Keithley 224 programmable current source and a Keithley 617 programmable electrometer) devices for measuring the electrical conductivity.

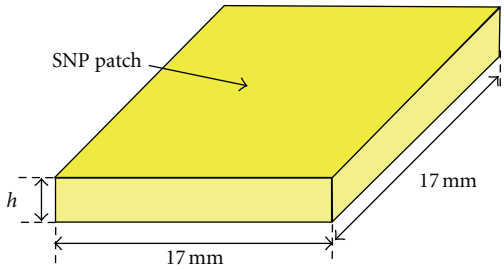

Figure 8: Sample of printed conductive SNP with its dimensions.

is a widely accepted approach for measuring the DC electrical resistivity of thin sheet samples [21]. A current source injects stable electrical current with a certain amount passing though the two outer probes. The voltage drop across the two inner probes can be measured using a voltmeter as can be seen in Figure 6. The electrical conductivity measurement is performed using Keithley 224 programmable current source and a Keithley 617 programmable electrometer as shown in Figure 7.

The measurement has been conducted using five printed samples of SNP ink with five different heights. The width and length of each sample fixed at 1.7 cm × 1.7 cm as shown in Figure 8. For each individual sample, we have considered two voltage readings, in the forward and reverse directions. Table 1 depicts the results of DC electrical conductivity from one to five layers of SNP patches. Ohm's law is used to calculate the DC electrical conductivity for the SNP ink using formula (1)

$$\rho = \frac{VWh}{IL^{-}}, \tag{1}$$

where ρ is the resistivity in ohm·m, V is the voltage measured by the voltmeter in volts, I is the current measured by the ammeter in amperes, W is the width of the sample bar measured in meters, h is the height of the sample bar measured in meters, and L^{-} is the distance between the two points where the voltmeter wires make constant to the bar measured in meters.

The measured DC electrical conductivity for the SNP ink is found to be around an average value of $(8.8 \pm 0.2) \times 10^4$ S/m. The small tolerance is due to the difficulty in obtaining two homogeneous current passages in two directions for the same SNP sample because of the cracks as can be seen in the SEM images in Figure 5.

The conductivity of printed SNP is lower than the bulk phase as a result of cracks, pores, surfactants and other impurities [22, 23]. This explains why the measured conductivity of printed SNP is less than that of bulk silver. The measured value of the electrical conductivity is used in CST MWS and HFSS to numerically evaluate the antenna performance.

4. Antenna Design and Simulation

As an example, the antenna is chosen to operate at a resonant frequency of 2.45 GHz since this band is very common and widely used in the wireless systems.

The transmission line model is used for calculating the dimensions of the patch. Three essential parameters, frequency of operation (f_o), height of dielectric substrate

Table 1: The DC electrical conductivity measurements.

No. of layers	Thickness/nm	Measured current/mA	Measured voltage/mV (forward)	Measured voltage/mV (reverse)	Conductivity/S/m
1	670	1.00	1.59	1.61	8.77×10^4
2	775	1.00	1.42	1.39	8.61×10^4
3	817	1.00	1.37	1.25	8.8×10^4
4	1100	1.00	1.02	1.00	8.5×10^4
5	1286	1.00	0.84	0.91	8.55×10^4

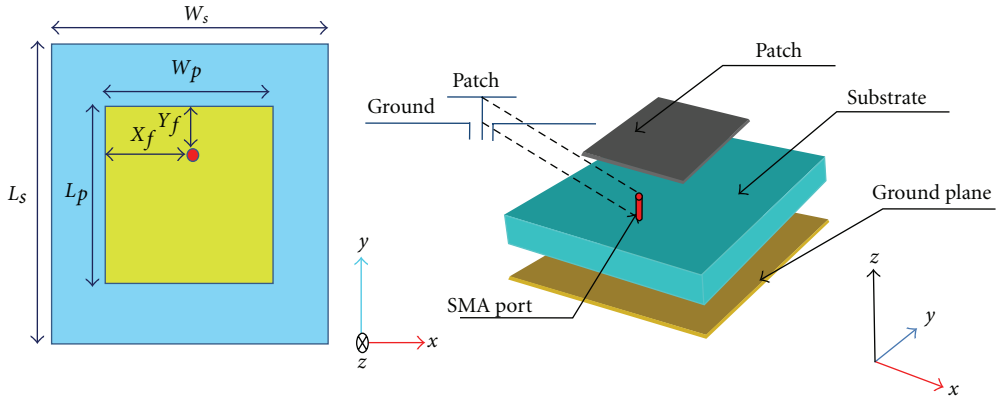

Figure 9: Geometry of the square patch antenna with the coaxial probe feed and the inset distances from the patch edge.

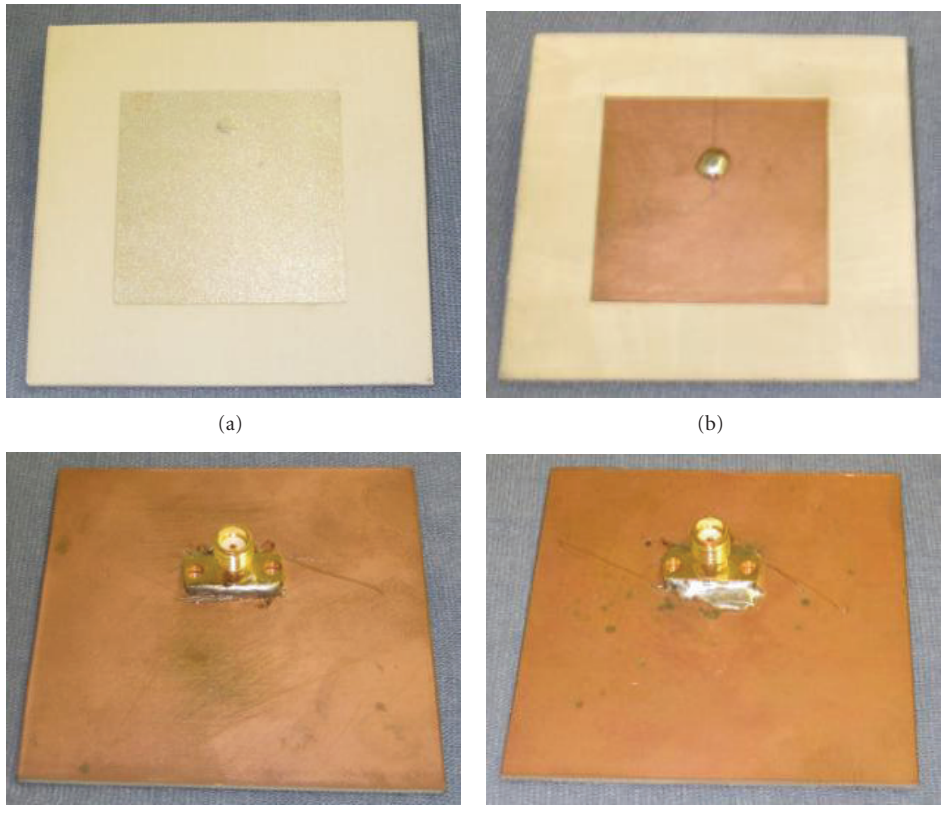

(a) (b)

(c) (d)

Figure 10: Prototype of the fabricated patch antenna (a) SNP, (b) copper, (c) and (d) the bottom view with SMA connector attached for SNP and copper, respectively.

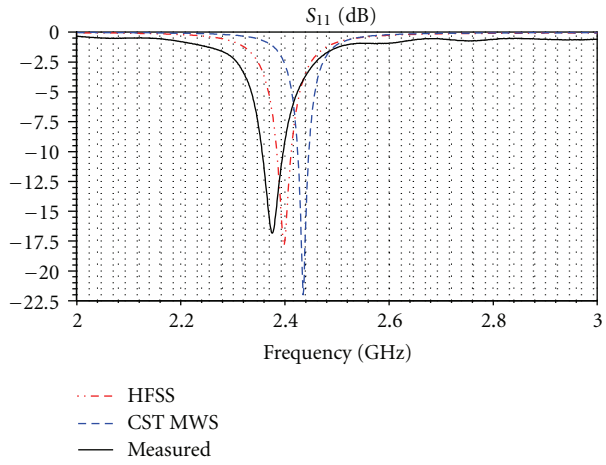

Figure 11: Comparison of S_{11} between CST, HFSS, and measurement of the square copper antenna.

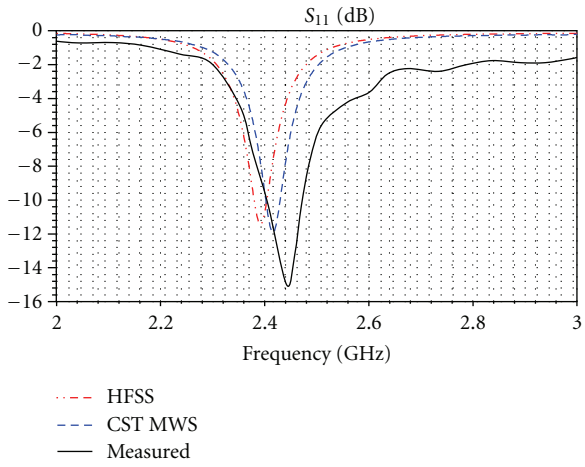

Figure 12: Comparison of S_{11} between CST, HFSS, and measurement of the SNP square patch.

Table 2: Dimensions of the square patch antenna.

Symbol	Parameter	Dimensions (mm)
L_p	Patch length	34.5
W_p	Patch width	34.5
L_s	Substrate length	60
W_s	Substrate width	60
X_f	Feed position in x direction	5.5
Y_f	Feed position in y direction	17.25

(h) and dielectric constant of the substrate, must be selected appropriately to design a microstrip patch antenna. The chosen substrate in this research is Rogers RO 3203 of a relative permittivity, ε_r, of 3.02, loss tangent, $\tan\delta = 0.0016$, and thickness of 1.524 mm. Using the equation

$$\varepsilon_{\text{reff}} = \frac{\varepsilon_{r+1}}{2} + \frac{\varepsilon_{r-1}}{2}\left[1 + \frac{12h}{W}\right]^{(-1/2)}, \tag{2}$$

Figure 13: Photograph of the radiation patterns measurement inside UALR's anechoic chamber.

the effective dielectric constant ($\varepsilon_{\text{reff}}$) is found as 2.826, and by applying the equation

$$\Delta L = 0.412h\frac{(\varepsilon_{\text{reff}} + 0.3)((W/h) + 0.264)}{(\varepsilon_{\text{reff}} - 0.258)((W/h) + 0.8)}, \tag{3}$$

the extension, ΔL, is found to be 0.746 mm. To calculate the effective length (L_{eff}), applying equation

$$(f_o)_{10} = \frac{c}{2(L + 2\Delta L)\sqrt{\varepsilon_{\text{reff}}}}, \tag{4}$$

we found L_{eff} to be equal to 36.41 mm. Using (4),

$$L_{\text{eff}} = L + 2\Delta L. \tag{5}$$

The length (L) is found as $L = 34.9$ mm.

The dimensions of the ground plane are determined by [24]

$$\begin{aligned} L_g &= 6h + L = 6(1.524) + 34.5 = 43.64\,\text{mm}, \\ W_g &= 6h + W = 6(1.524) + 34.5 = 43.64\,\text{mm}. \end{aligned} \tag{6}$$

However, the design of the square microstrip antenna is based on a larger ground plane (60 mm × 60 mm) to reduce the level of side lobes. The feed point must be located where the input impedance is 50 ohms at the resonant frequency. The location of the feeding point is achieved by a trial-and-error method by selecting a distance 30% from the edge and moving is a small step to ($X_f = 5.5$ mm, $Y_f = 17.25$ mm), locate the optimum feed point where the S_{11} is minimum.

In Figure 9, the geometrical details of the square patch are shown.

As illustrated in Figure 9, the dimensions of $L_p \times W_p$ for the microstrip patch and for the substrate, $L_s \times W_s$, are illustrated in Table 2.

These antenna parameters in addition to the electrical conductivity discussed in the previous section are then fed to two simulation software based on two different techniques, Finite Integration Technique (FIT) of CST Microwave Studio (CST MWS) and the Finite Element Method (FEM) formulation of Ansoft's High Frequency Structure Simulator (HFSS), which are chosen for validation purposes. In the next section, the simulation results of both softwares are compared to the measured ones.

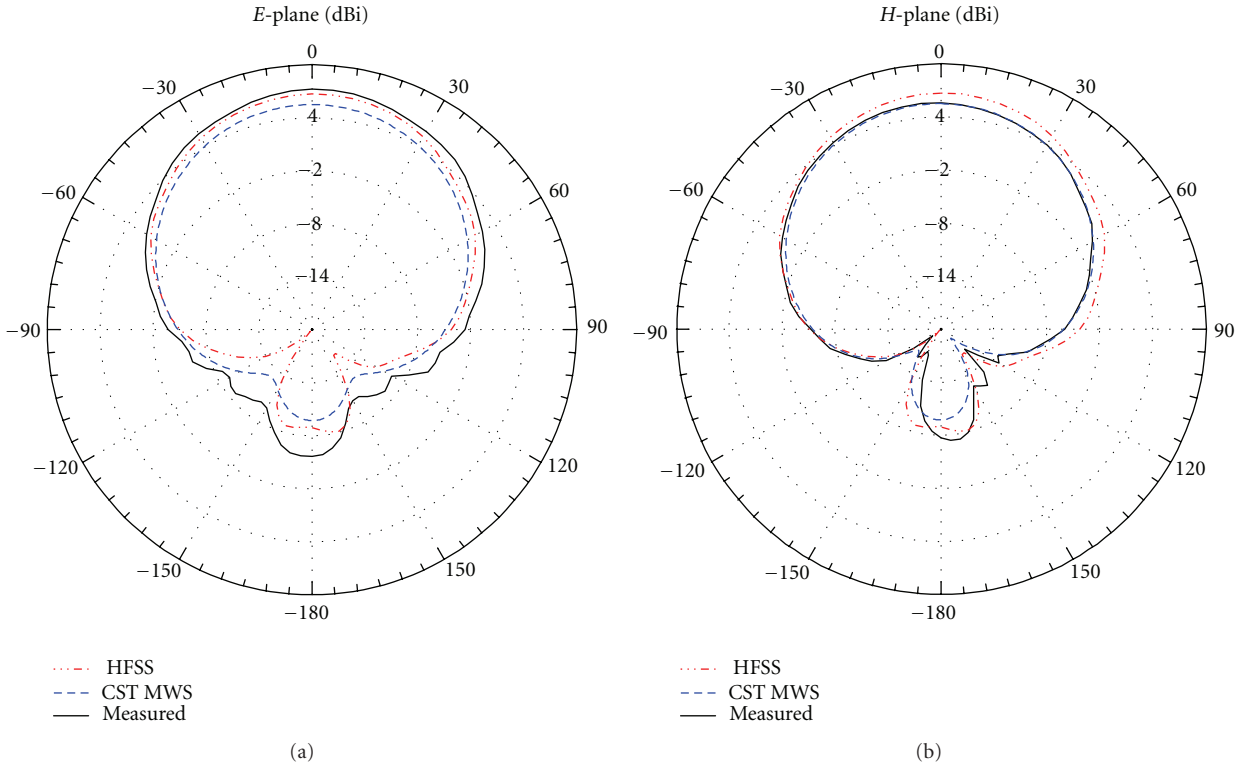

Figure 14: Simulated and measured far-field radiation patterns in the (a) E-plane and (b) H-plane for the copper antenna at $f_o = 2.45$ GHz.

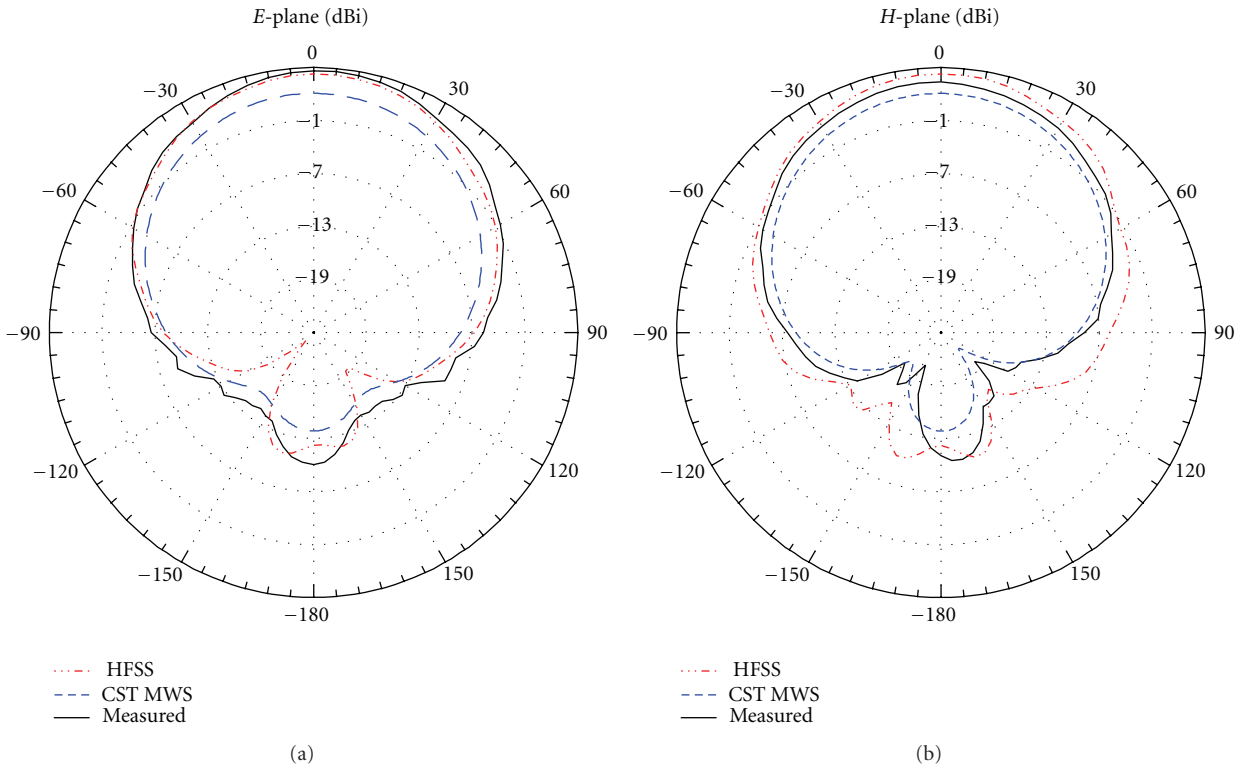

Figure 15: Simulated and measured far-field radiation patterns in the (a) E-plane and (b) H-plane for the SNP antenna at $f_o = 2.45$ GHz.

Table 3: Tabulated comparison of the experimental and simulated results.

	Copper			Sliver		
	Simulation		Measured	Simulation		Measured
	CST	HFSS		CST	HFSS	
f_o/GHz	2.43	2.39	2.37	2.41	2.39	2.44
S_{11}/dB	−22	−17.8	−16.8	−11.9	−11.41	−15.2
Bandwidth/MHz (S_{11} is −10 dB or lower)	22	28	41	26	63	80
Bandwidth %	9.03	11.6	14.8	10.7	26.3	32.7
f_o Shift %	2.4	0.92	—	1.18	2.16	—
Gain/dB	6.3	6.7	5.9	5	5.3	4.6

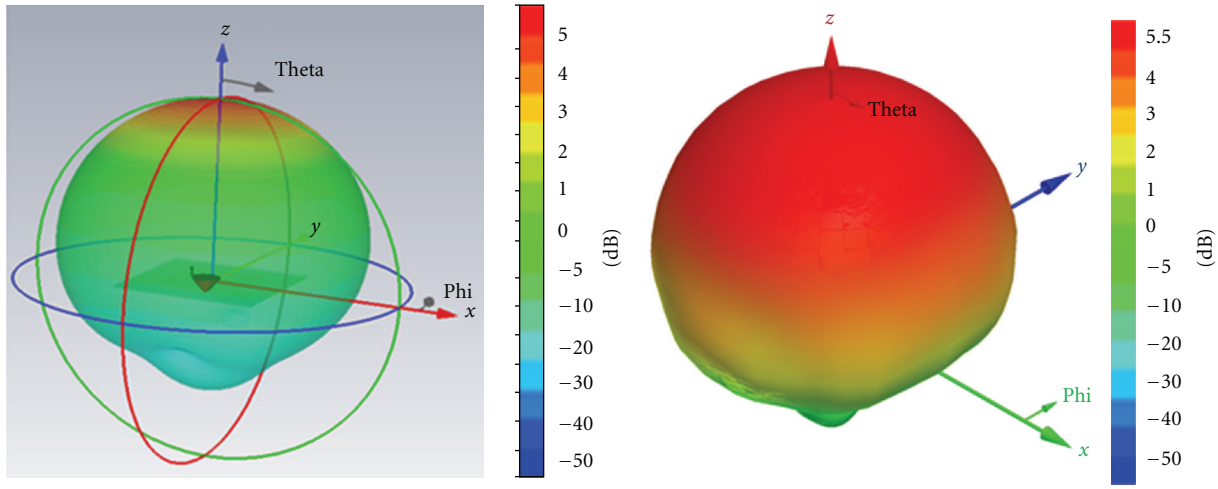

(a) (b)

Figure 16: Radiation patterns of SNP antenna evaluated using (a) CST MWS and (b) HFSS.

5. Fabrication and Measurement

After exporting the Gerber file of the simulated design to the printer, loading the substrate and adjusting the nozzles distances as discussed previously, the printing order is given to print the SNP-based square patch. Next, thermal curing is applied and feed is applied afterwards. A coaxial feed is used to excite the microstrip antenna using a microdriller, silver paste, and soldering station to fix the 50 ohm subminiature version A (SMA) port. The SMA is connected to the antenna by carefully drilling the antenna at the specified position. The inner conductor of the coaxial cable is connected and soldered to the patch, and the outer conductor of the coaxial cable is soldered to the ground plane. The inner conductor of the SMA port is connected to the patch through the substrate using silver paste while the inner conductor of the SMA is soldered to the copper patch. For both patches, the SMA port is soldered to their ground plane.

For comparison purposes, the printed prototype is compared to an identical prototype made out of copper using a traditional photolithography technique. The SNP antenna and its identical copper prototype are shown in Figure 10.

The measurement of S_{11} is performed using an Agilent E5071B Vector Network Analyzer (VNA). The VNA is calibrated using short −50 Ω load-open circuit caliper kit. The test is performed within the 2 GHz to 3 GHz band. The antenna is connected to the VNA through a 50 Ω coaxial cable and set on a foam box to avoid the near-field interactions.

A good agreement between the simulated and measured S_{11} has been achieved for copper and SNP prototypes as can be seen in Figures 11 and 12, respectively. A slight shift in the resonant frequency has been observed around the design frequency 2.45 GHz for both the SNP and copper prototypes. The discrepancies between the measured and simulated f_o and bandwidth are attributed to the unavoidable manufacturing tolerances, in particular the feed structure.

The measured and simulated results for the SNP and copper prototypes are listed in Table 3.

The far-field radiation patterns are measured at the resonant frequency in the E-plane and H-plane for the SNP and copper antennas inside the University of Arkansas at Little Rock (UALR) anechoic chamber, which is shown in Figure 13.

The simulated and measured radiation patterns for the E-plane and H-plane show a good agreement as can be seen in Figures 14 and 15, respectively. The gain evaluated of the copper patch antenna from CST MW at 2.43 GHz is

6.3 dB, and the gain at the resonant frequency of 2.39 GHz is 6.7 dB from HFSS. The measured gain is 5.9 dB at 2.37 GHz as depicted in Figure 14. Furthermore, the gain of the SNP patch antenna obtained from CST is 5 dB at 2.41 GHz and 5.3 dB at 2.39 GHz from HFSS. However, the measured gain is 4.6 dB at 2.44 GHz as shown in Figure 15.

The 3D radiation patterns evaluated from CST MWS and HFSS for the SNP patch antenna are shown in Figure 16.

6. Conclusions

In this paper, a systematic approach for the design, fabrication, and testing of microstrip antennas using IJPT is presented. A conventional antenna design based on the square patch geometry is adopted in this research as a benchmark, which could be applied to different complex geometries. The systematic approach for the fabrication process includes the optimal number of printed layers, curing temperature, and curing time, to achieve high electrical conductivity. The antenna is fabricated using DMP-2800 Dimatix FujiFilm Material Printer and SNP ink. To conclude, this study provides the antenna community with an easy-to-follow optimized systematic methodology for producing microstrip antennas using inkjet printing technology.

References

[1] A. Rida, L. Yang, and M. M. Tentzeris, "Design and characterization of novel paper-based inkjet-printed UHF antennas for RFID and sensing applications," in *Proceedings of the IEEE Antennas and Propagation Society International Symposium (AP-S '07)*, pp. 2749–2752, June 2007.

[2] L. Yang and M. M. Tentzeris, "Design and characterization of novel paper-based inkjet-printed RFID and microwave structures for telecommunication and sensing applications," in *Proceedings of the IEEE MTT-S International Microwave Symposium (IMS '07)*, pp. 1633–1636, June 2007.

[3] Z. Konstas, A. Rida, R. Vyas, K. Katsibas, N. Uzunoglu, and M. M. Tentzeris, "A novel "Green" inkjet-printed Z-shaped monopole antenna for RFID applications," in *Proceedings of the IEEE 3rd European Conference on Antennas and Propagation (EuCAP '09)*, pp. 2340–2343, March 2009.

[4] A. Rida, L. Yang, T. Reynolds, E. Tan, S. Nikolaou, and M. M. Tentzeris, "Inkjet-printing UHF antenna for RFID and sensing applications on liquid crystal polymer," in *Proceedings of the IEEE International Symposium on Antennas and Propagation and USNC/URSI National Radio Science Meeting (APSURSI '09)*, pp. 1–4, June 2009.

[5] A. Traille, L. Yang, A. Rida, T. Wu, and M. M. Tentzeris, "Design and modeling of novel multiband/wideband antennas for RFID tags and readers using time/frequency-domain simulators," in *Proceedings of the Workshop on Computational Electromagnetics in Time-Domain (CEM-TD '07)*, pp. 1–3, October 2007.

[6] D. E. Anagnostou, A. A. Gheethan, A. K. Amert, and K. W. Whites, "A direct-write printed antenna on paper-based organic substrate for flexible displays and WLAN applications," *Journal of Display Technology*, vol. 6, no. 11, pp. 558–564, 2010.

[7] V. K. Palukuru, A. Pekonen, V. Pynttäri, R. Mäkinen, J. Hagberg, and H. Jantunen, "An inkjet-printed inverted-F antenna for 2.4-GHz wrist applications," *Microwave and Optical Technology Letters*, vol. 51, no. 12, pp. 2936–2938, 2009.

[8] L. Yang, R. Zhang, D. Staiculescu, C. P. Wong, and M. M. Tentzeris, "A novel conformal RFID-enabled module utilizing inkjet-printed antennas and carbon nanotubes for gas-detection applications," *IEEE Antennas and Wireless Propagation Letters*, vol. 8, pp. 653–656, 2009.

[9] S. Merilampi, L. Ukkonen, L. Sydanheimo, P. Ruuskanen, and M. Kivikoski, "Analysis of silver ink bow-tie RFID tag antennas printed on paper substrates," *International Journal of Antennas and Propagation*, vol. 2007, Article ID 90762, 9 pages, 2007.

[10] L. Yang, R. Vyas, A. Rida, J. Pan, and M. M. Tentzeris, "Wearable RFID-enabled sensor nodes for biomedical applications," in *Proceedings of the 58th Electronic Components and Technology Conference (ECTC '08)*, pp. 2156–2159, May 2008.

[11] M. M. Tentzeris, "Novel paper-based inkjet-printed antennas and wireless sensor modules," in *Proceedings of the IEEE International Conference on Microwaves, Communications, Antennas and Electronic Systems (COMCAS '08)*, pp. 1–8, May 2008.

[12] Y. Amin, J. Hallstedt, H. Tenhunen, and L. R. Zheng, "Design of novel paper-based inkjet printed rounded corner bowtie antenna for RFID applications," *Sensors & Transducers Journal*, vol. 115, no. 4, pp. 160–167, 2010.

[13] L. Yang, A. Rida, T. Wu, S. Basat, and M. M. Tentzeris, "Integration of sensors and inkjet-printed RFID tags on paper-based substrates for UHF "cognitive intelligence" applications," in *Proceedings of the IEEE Antennas and Propagation Society International Symposium (AP-S '07)*, pp. 1193–1196, June 2007.

[14] L. Yang, L. Martin, D. Staiculescu, C. P. Wong, and M. M. Tentzeris, "Design and development of compact conformal RFID antennas utilizing novel flexible magnetic composite materials for wearable RF and biomedical applications," in *Proceedings of the IEEE International Symposium on Antennas and Propagation and USNC/URSI National Radio Science Meeting (APSURSI '08)*, pp. 1–4, July 2008.

[15] V. Pynttäri, R. Mäkinen, J. Lilja, V. Pekkanen, P. Mansikkamäki, and M. Kivikoski, "Significance of conductivity and thickness of thin inkjet printed microstrip lines," in *Proceedings of the 12th IEEE Workshop on Signal Propagation on Interconnects*, pp. 1–4, May 2008.

[16] "Computer simulation technology/ microwave studio CST MWS," 2011, http://www.cst.com/.

[17] "Ansoft's high frequency structure simulator HFSS," Version 13, 2011, http://www.ansys.com/.

[18] http://www.fujifilmusa.com/products/industrial_inkjet_printheads/index.html.

[19] A. Rida, L. Yang, R. Vyas, S. Basat, S. K. Bhattacharya, and M. M. Tentzeris, "Novel manufacturing processes for ultra-low-cost paper-based RFID tags with enhanced 'wireless intelligence'," in *Proceedings of the 57th Electronic Components and Technology Conference (ECTC '07)*, pp. 773–776, June 2007.

[20] A. Rida, S. Nikolaou, and M. M. Tentzeris, "Broadband UHF RFID/sensor modules for pervasive cognition applications," in *Proceedings of the 3rd European Conference on Antennas and Propagation (EuCAP '09)*, pp. 2344–2347, March 2009.

[21] N. D. Robinson and M. Berggren, *Handbook of Conducting Polymers*, 3rd edition, 2007.

[22] T. H. J. van Osch, J. Perelaer, A. W. M. de Laat, and U. S. Schubert, "Inkjet printing of narrow conductive tracks on untreated polymeric substrates," *Advanced Materials*, vol. 20, no. 2, pp. 343–345, 2008.

[23] M. Mantysalo and P. Mansikkamaki, "An inkjet-deposeted antenna for 2.4 GHz applications," *International Journal of Electronics and Commnuications*, vol. 63, no. 1, pp. 31–35, 2009.

[24] C. A. Balanies, *Antenna Theory: Analysis & Design*, John Wiley & Sons, 1997.